Int. J. Therm. Sci. (2001) 40, 724–737

S1290-0729(01)01261-3/FLA

Melting characteristics of ice water slurry by warm air bubbling

Shigeo Aoyama [a*], Hideo Inaba [b]

[a] *Refrigeration Research Laboratory, Matsushita Refrigeration Company, 4-2-5 Takaida Hondori, Higashi-Osaka, Osaka 577-8501, Japan*
[b] *Department of Mechanical Engineering, Okayama University, 3-1-1 Tsushima-naka, Okayama 700-8530, Japan*

(Received 22 May 2000, accepted 4 October 2000)

Abstract — This paper has dealt with direct contact heat exchange characteristics between ice water slurry (average ice particle diameter: 3.10 mm) and warm air bubbles as a heat transfer medium. The warm air bubbles ascending in the layer fluidized the ice water slurry layer, and the bubbles were cooled down directly by the ice water slurry. The following results were obtained from the experiment. In case of ice water slurry layer, the warm air bubbles fluidized the layer in earlier stage and heat exchange performance was higher than using ice particles layer. The maximum temperature efficiency increased as Reynolds number Re increased because fluidity in the layer became active and kept at the fixed value in the region of $Re \geq 900$. Dehumidity efficiency increased as modified Stefan number and Re increased since the heat capacity of inlet air and heat transfer coefficient increased. Some empirical correlations for temperature efficiency, dehumidity efficiency and the completion time of melting were derived in terms of various nondimensional parameters. © 2001 Éditions scientifiques et médicales Elsevier SAS

ice water slurry / moist air / packed bed / direct contact heat exchange / temperature efficiency / dehumidity efficiency / melting characteristics

Nomenclature

a_a	thermal diffusivity of air	$m^2 \cdot s^{-1}$
c_{pa}	specific heat at constant pressure of air	$kJ \cdot kg^{-1} \cdot K^{-1}$
c_{ps}	specific heat at constant pressure of vapor	$kJ \cdot kg^{-1} \cdot K^{-1}$
d_n	nozzle diameter of the dispersion plate	m
d_{ice}	average diameter of ice particle	m
h_a	specific enthalpy of air	$kJ \cdot kg^{-1}$
L	latent heat of ice melting $= 334.88\ kJ \cdot kg^{-1}$	$kJ \cdot kg^{-1}$
m_i	mass of ice particles	kg
m_w	mass of water	kg
Q_a	time integrated value of the total transmitted heat between ice water slurry and air	kJ
Q_c	time integrated value of condensed heat exchange quantity of vapor in air bubbles	kJ
Q_{ice}	latent heat of ice water slurry layer	kJ
Q_{loss}	time integrated value of heat loss of ice water slurry layer	kJ
Q_s	time integrated value of sensible heat exchange quantity of dry air in air bubbles	kJ
Q_{total}	time integrated value of the total transmitted heat in the ice water slurry layer	kJ
Re	Reynolds number	
r	specific latent heat of condensation of vapor	$kJ \cdot kg^{-1}$
Ste_h	modified Stefan number	
T	temperature	°C
T_{btm}	temperature on the dispersion plate	°C
T_c	temperature in the ice water slurry layer	°C
T_m	melting point of ice = 0 °C	°C
t	time	s
t_l	completion time of melting	s
t_l^*	nondimensional completion time of melting	s
U_n	air flow velocity in nozzle outlet	$m \cdot s^{-1}$
v	specific volume	$m^3 \cdot kg^{-1}$
V_a	volumetric flow rate of air	$Nm^3 \cdot s^{-1}$
x	absolute humidity	$kg \cdot kg^{-1}$
x_s	saturated absolute humidity	$kg \cdot kg^{-1}$
x_o	absolute humidity of dry air	$kg \cdot kg^{-1}$
Δx_a	absolute humidity difference between the inlet air and outlet air of test section	$kg \cdot kg^{-1}$

* Correspondence and reprints.
E-mail addresses: aoyama@mrc.mei.co.jp (S. Aoyama), inaba@mech.okayama-u.ac.jp (H. Inaba).

Z	initial packing height of ice water slurry layer	m
Z^*	nondimensional height of ice water slurry layer	

Greek Symbols

β	ice packing factor $= m_i/(m_i + m_w)$	
ε	humidifying efficiency $= 1 - x_{aout}/x_{ain}$	
θ	maximum temperature efficiency $= (T_{ain} - T_{aout})/(T_{ain} - T_m)$	
ϕ	relative humidity	%
ν_a	kinematic viscosity of air	$m^2 \cdot s^{-1}$
Φ_a	transmitted heat between ice water slurry and air	kW
Φ_c	latent heat of condensation of vapor in air bubbles	kW
Φ_s	sensible heat of dry air in air bubbles	kW
Φ_{loss}	heat loss of ice water slurry layer	kW
Φ_{total}	total heat transmitted heat in the ice water slurry layer	kW

Subscripts

ain	inlet air
aout	outlet air

1. INTRODUCTION

Recently, ice thermal storage systems using nighttime electric power have been widely developed in order to cope with rapid increase in demand for daytime electric power, and ice thermal storage systems thus developed are used for air conditioning of buildings in Japan. And, instead of a water transportation system that runs in cooling mode, carrying cold water obtained by heat exchange between water and ice in a thermal storage tank, to indoor air conditioner, an ice water transportation system that directly carries ice water slurry through pipe lines to indoor side air conditioner has been studied and developed [1, 2].

By supplying latent heat of ice to the indoor side of air conditioning unit, the ice water transportation system is able to remarkably increase thermal energy carrying quantity per unit flow rate as compared to a the cold water transportation system. Therefore, reduction in piping diameter and pump power can be achieved in the ice water transportation system. Furthermore, in addition to the ice water transportation system, a method for cooling hot water flowing in outer tube of double tube heat exchanger is proposed, wherein ice water slurry flows into the inner tube of double tube heat exchanger [3]. Also proposed is a method for cooling by direct contact heat exchange between air and ice cube after carrying the ice cube to packed bed [4]. Technology of direct contact heat exchange between air bubbles and latent heat storage material has been studied, in which various latent heat storage materials serve as heated mediums and air bubbles as heating mediums [5–7]. In the above-mentioned direct contact heat exchange, since injected air bubbles fluidize the latent heat storage material, it is advantageous in that the temperature field of the latent heat storage material becomes uniform and uniform heat exchange takes place between latent heat storage material and air bubbles. However, the study on the melting characteristics of direct contact heat exchange between ice water and air has not been made. The melting system by direct contact heat exchange between ice water and warm air has advantages that it can be simultaneously cooled and dehumidified because of not only cooling warm air by ice water, but also condensing the steam in warm air by ice water in latent heat exchange.

This paper refers to the experimental study on the ice melting behavior and the heat exchange characteristics of passing air and ice water slurry. Air bubbles are generated by air passing through a dispersion plate with many circular nozzles evenly arranged at the bottom of ice water slurry layer. The air bubbles are injected into the layer from the nozzles in order to perform direct contact heat exchange with the ice water slurry. The heat transfer characteristics vary with the mixing ratio of ice particles and water or the passing airflow rate etc. In the present study, it is intended to examine experimentally the effects of the experimental factors such as inlet air temperature, humidity, and airflow rate and ice packing factor on outlet air temperature, humidity and completion time of melting. Further, it is intended to sum up the correlation in the form of empirical equations.

2. EXPERIMENTAL APPARATUS AND METHOD

The experimental apparatus consists of the test section and warm air supplying line as shown in *figure 1(a)*. The air is delivered by the compressor and goes to the volume flow meter through the buffer tank, constant-pressure valve and flow rate adjusting needle valve. And the air coming out of the volume flow meter is branched into the air that goes to the heater from the bubble tower humidifier through the flow rate adjusting needle valve and the air that directly goes to the heater, bypassing the bubble tower humidifier, and then flows into the bottom of the test section with the temperature and humidity adjusted to the set-points. The test section, as shown in

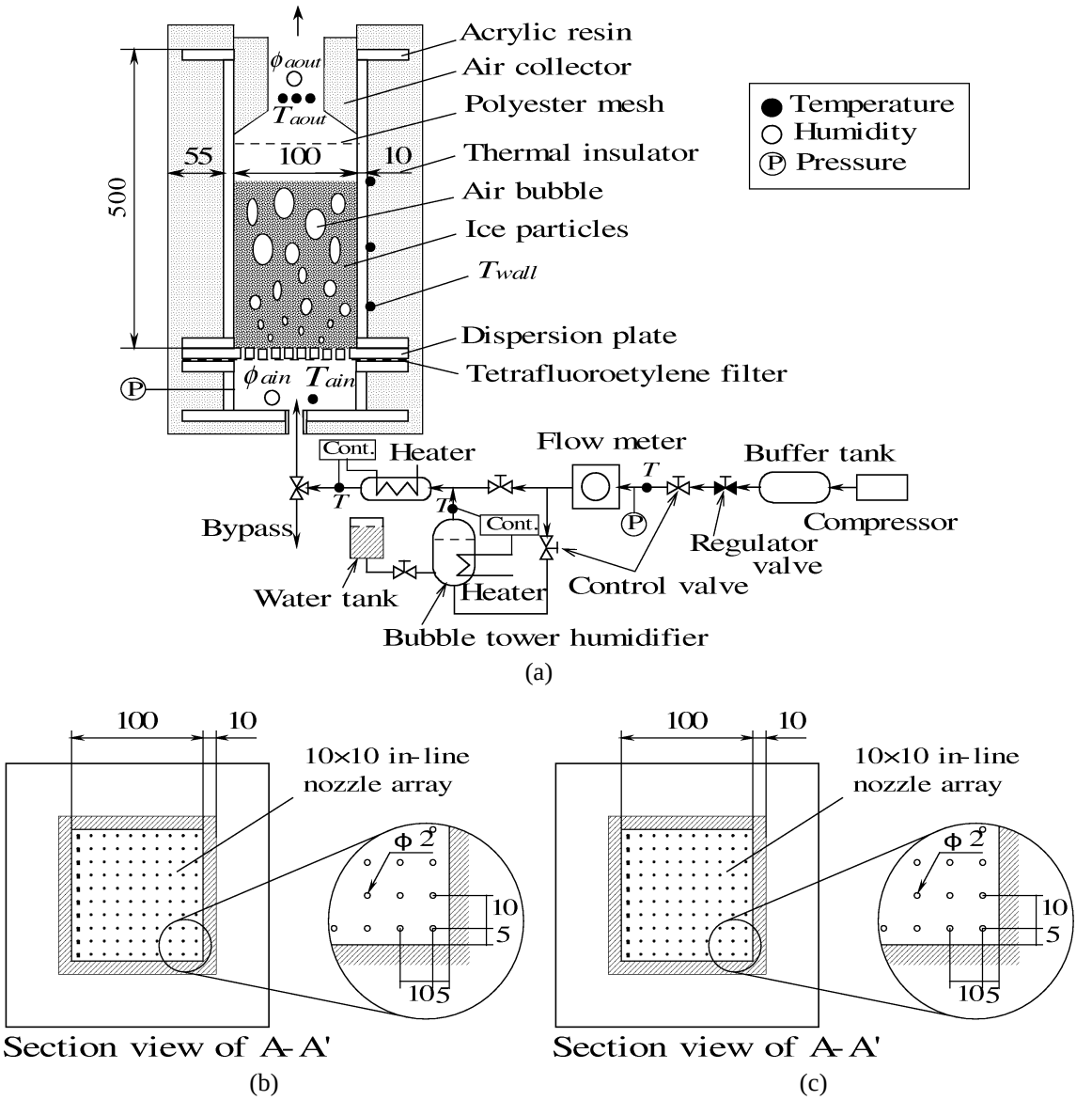

Figure 1. Schematic diagram of experimental apparatus. (a) Experimental apparatus. (b) Dispersion plate. (c) Measuring position of temperature.

figure 1(a), is an upright rectangular duct whose internal section is 100 mm × 100 mm, 500 mm in height, which is made of clear acrylic resin plate of 10 mm in thickness.

The inlet air temperature T_{ain} and inlet relative humidity ϕ_{ain} of the air flowing into the bottom of the test section are respectively measured by a platinum resistance thermometer and hygrometer (polymer film type, measuring range: 0–100 RH%, measuring accuracy: ±3 RH%). After that, the air is injected into the ice water slurry layer through the dispersion plate at the bottom of the test section.

The ice water slurry is the mixture of ice particles and water, and the injected air turns into bubbles. The bubbles ascend up in the ice water slurry layer during exchanging heat with ice water slurry. And the air flowing out of the ice water slurry layer is agitated in the throttle duct made of foamed styrol thermal insulator that is located at the layer top. Then, the outlet mixture average temperature

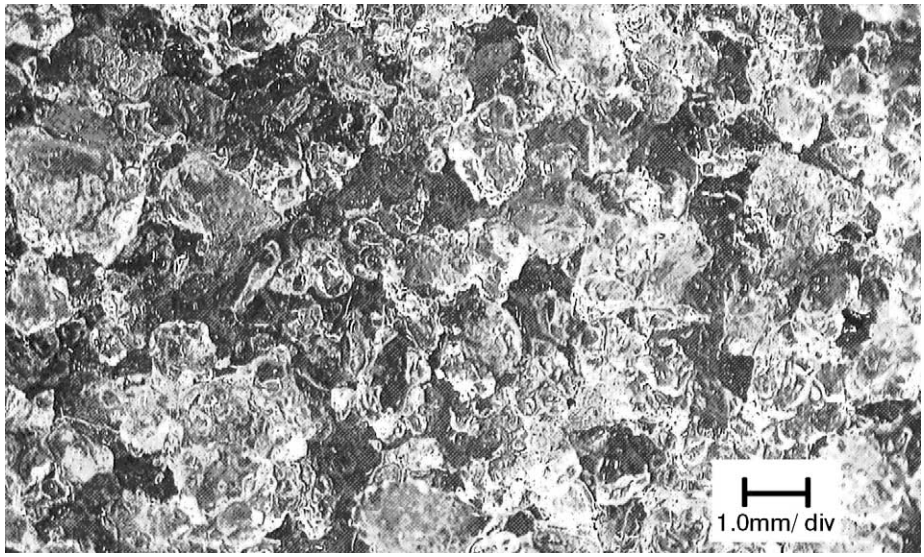

Figure 2. Ice particles.

T_{aout} and the outlet relative humidity ϕ_{aout} of the air are respectively measured by the multiple thermocouples and hygrometers that are installed inside the duct. The throttle duct is provided with polyester mesh (40 meshes) at the bottom in order to prevent the ice water spattered from the ice water slurry layer from sticking to the thermocouples or hygrometers located inside the throttle duct. Also, bubbles are generated in the upper surface of ice water slurry, while the air is flowing upward and at the same time the bubble layer height varies with the lapse of time. So, the throttle duct equipped with thermocouples and hygrometers is designed so that it is able to move up and down as needed and to measure the temperature and humidity of the air just after passing through the ice water slurry at all times.

As shown in *figure 1(b)*, the dispersion plate is made of clear acrylic resin plate of 10 mm thickness on which circular nozzles with diameter d_n ($= 2 \times 10^{-3}$ m) are arranged in 100 checkerboard pattern at 10 mm intervals. And a tetrafluoroethylene filter (thickness: 0.54 mm, effective retention size: 2 μm, porosity ratio: 54%) is installed under the dispersion plate so that the water in the test section does not leak below the filter even when the air does not flow into the test section. The nozzle diameter has been set from the points that the ice particles ($\overline{d}_{ice} = 3.10$ mm) *should not be put into the nozzles*, the initial diameter of the produced bubbles should be equal to or smaller as compared with the ice particles and that pressure drop in the dispersion plate should be reduced to a minimum. The nozzle intervals have been set from the points that the generated bubbles should efficiently heat-exchange with the ice water slurry while they are sufficiently stirred in the ice water slurry layer without combining with one another just after flowing out of the nozzles. Also, it has been confirmed by visualized observation that the air bubbles generated from each nozzle on the dispersion plate are nearly uniform and that air bubble generating system can be created in limitless area by the experimental apparatus. *Figure 1(c)* shows the position of the thermocouples in the test section. As shown in this figure, two thermocouples are installed 20 mm above the dispersion plate to measure the average temperature of these two thermocouples as the characteristic temperature T_c in the ice water slurry. Also, a thermocouple is affixed to the dispersion plate to measure the temperature T_{btm} at the bottom of ice water slurry layer. All the thermocouples used in the test section are T type with strand diameter 0.32 mm and measuring accuracy ±0.5 K.

Figure 2 is the appearance of the ice particles used in the experiment, showing that the ice particles are rather oval-shaped. *Figure 3* shows the diameter distribution of the average diameter d_{ice} of long and short diameters of the ice particles used in the experiment, and shows that the mathematical average diameter of ice particles is $\overline{d}_{ice} = 3.10$ mm.

Also, regarding the measurement of the initial packing height Z just after packing the ice water slurry into the test section, the average value can be obtained because

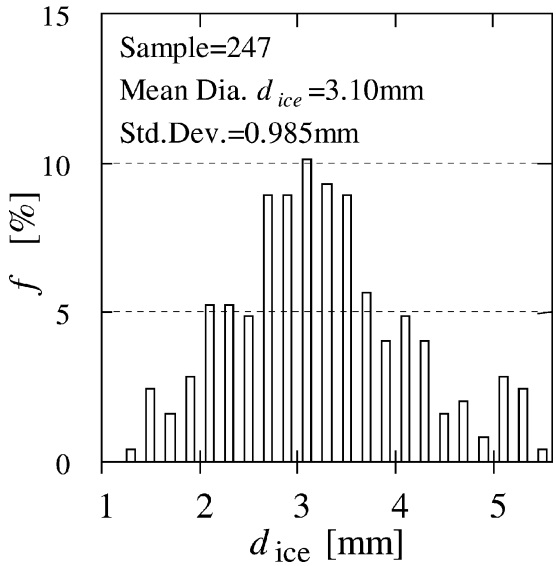

Figure 3. Diameter distribution of ice particles.

TABLE I
Experimental condition.

Mass of ice particles	m_{i}	: 0.12–0.53	kg
Mass of water	m_{w}	: 0–1.51	kg
Ice Packing Factor	β	: 0.15–1.00	
Layer height	Z	: 0.05–0.21	m
Volumetric air flow rate	V_{a}	: $(0.67–3.17)\cdot10^{-3}$	$\mathrm{Nm^3\cdot s^{-1}}$
Inlet air temperature	T_{ain}	: 30–46	°C
Inlet air relative humidity	ϕ_{ain}	: 7–87	%
Inlet air absolute humidity	x_{ain}	:0.004–0.046	$\mathrm{kg\cdot kg^{-1}}$

the ice water slurry layer surface was not completely flat but irregular (measurement error: ±2.5 mm).

The parameters of the experimental conditions are ice packing factor β calculated by mass of ice particles m_{i} and mass of water m_{w}, the initial layer height Z of ice particles layer and ice water slurry layer, the volumetric airflow rate V_{a}, the inlet air temperature T_{ain}, and the inlet air relative humidity ϕ_{ain} (absolute humidity x_{ain}). The experimental conditions of parameters are shown in *table I*.

At this point, the pressure drop of air in ice water slurry is not so high. The pressure drop of air in the ice water slurry is, for example, about 0.2–1.1 kPa {20–115 mmAq} when volumetric airflow rate V_{a} is $1.67\cdot10^{-3}$ $\mathrm{m^3\cdot s^{-1}}$. This means that the pressure drop of air in ice water slurry almost depends on the pressure head of water, which is about half of the initial packing height Z of ice water slurry layer, in all the ice water slurry melting. This is because the airflow velocity in the layer is very slow and also the appearance of influence by buoyancy of air bubbles in the layer.

3. EXPERIMENTAL RESULTS AND CONSIDERATION

3.1. Fluidization of ice particles layer and air bubbles

The photo-view of melting process (a) and the schematic figure of melting condition (b) that represents the tendency of ice particles layer melting behavior are shown in *figure 4* with respect to melting behavior of the ice particles layer by injected warm air when only the ice particles layer (ice packing factor $\beta = 1.0$) is packed into the test section. The mechanism of heat transfer in melting of the ice particles layer by warm air is as follows. The air bubbles come in contact with the ice particles in the ice particles layer and then the vapor in the air bubbles is condensed thereby producing condensed water to discharge the latent heat of condensation Φ_{c}. Simultaneously the melted water of ice particles and the dry air in the air bubbles contacting with the aforementioned condensed water are cooled to discharge the sensible heat Φ_{s}. That is, the air bubbles discharge the sensible heat Φ_{s} into the ice particles layer and at the same time discharge the latent heat of condensation Φ_{c} of the vapor, and therefore cooling and dehumidifying of air bubbles are simultaneously performed.

In the beginning of melting process, as shown in *figure 4(a(1))* and *figure 4(b(1))*, the whole layer does not start fluidizing even with warm air flowing through the ice particles layer. Therefore, volume of water and passage of air bubbles are not enough to fluidize the whole layer. Subsequently, at the initial stage of melting process (*figure 4(a(2))*), as shown in *figure 4(b(2))*, melting of the ice particles layer occurs at bottom of the ice particles layer (warm air inlet side) and the water (melted water + condensed water) begins to increase. And while the warm air pushes up the ice particles layer to the top, the fluidity is not enough to agitate the whole ice particles layer, because the ice particles layer containing some water remains at the upper part of the layer (warm air inlet side).

After that, as shown in *figure 4(a(3))* and *figure 4(b(3))*, melting of the ice particles gradually takes place at the

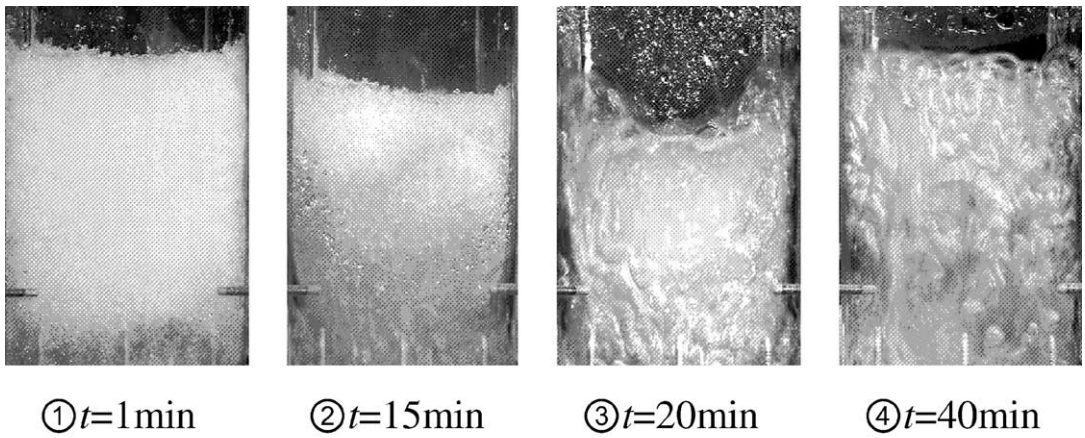

V_a=0.733×10^{-3}Nm^3/s, T_{ain}=42.7ºC, ϕ_{ain}=39.9%, x_{ain}=0.0210kg/kg'

m_i=0.51kg , m_w=0kg , Z=0.110m

(a)

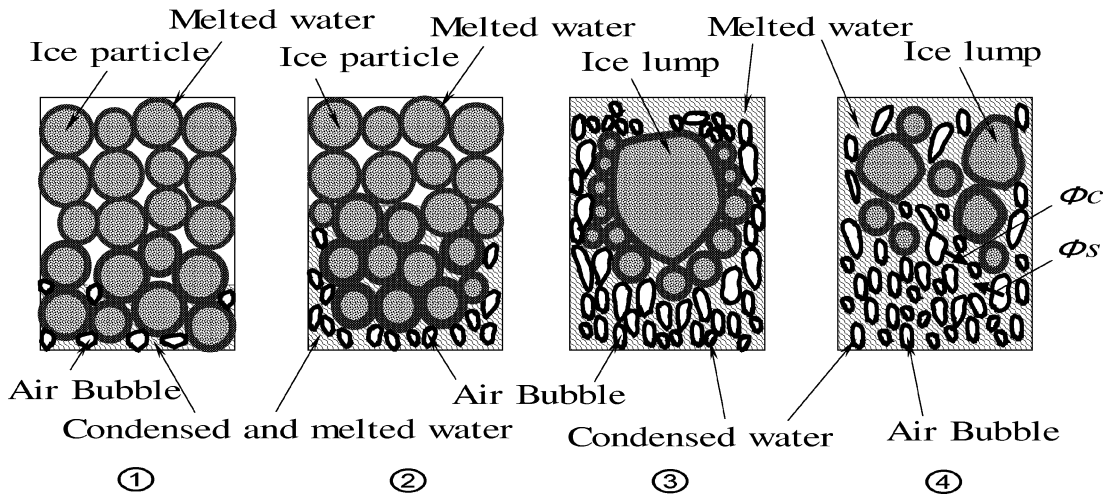

(b)

Figure 4. Melting behavior of ice particles. (a) View of melting process. (b) Schematic figure of melting condition.

lower part of the layer, and the remaining ice particles move together and change to several large lumps. Then, the air bubbles combine with one another to wrap up the lumps up and change to large air bubbles. And the ice water slurry layer is entirely fluidized. At the final stage of melting (*figure 4(a(4))*), as shown in *figure 4(b(4))*, melting further takes place almost equally over the whole ice water slurry layer and the increase in the volume of water promotes the fluidization of ice water slurry layer. Finally the remaining ice particles disappear and change into liquid phase and the melting process is completed.

As stated above, when warm air is injected into only the ice particles layer (ice packing factor $\beta = 1.0$), there is no fluidity over the whole layer because of little water at the initial stage of melting, and as a result, it has been confirmed that the heat exchange between ice particles layer and warm air is low in performance at the initial stage of melting.

3.2. Fluidization of ice water slurry layer and air bubbles

The photo-view of melting process (a) and the schematic figure of melting condition (b) are shown in *figure 5* with respect to the melting behavior of ice water slurry layer by injected warm air when the ice water slurry layer (ice packing factor $\beta = 0.5$) is packed into the test section. The mechanism of heat transfer in the melting phenomenon of the ice water slurry layer due to warm air is basically the same as in the case of packing only ice particles layer. As shown in *figure 5(b)*, the vapor in air bubbles is condensed due to the low temperature water in

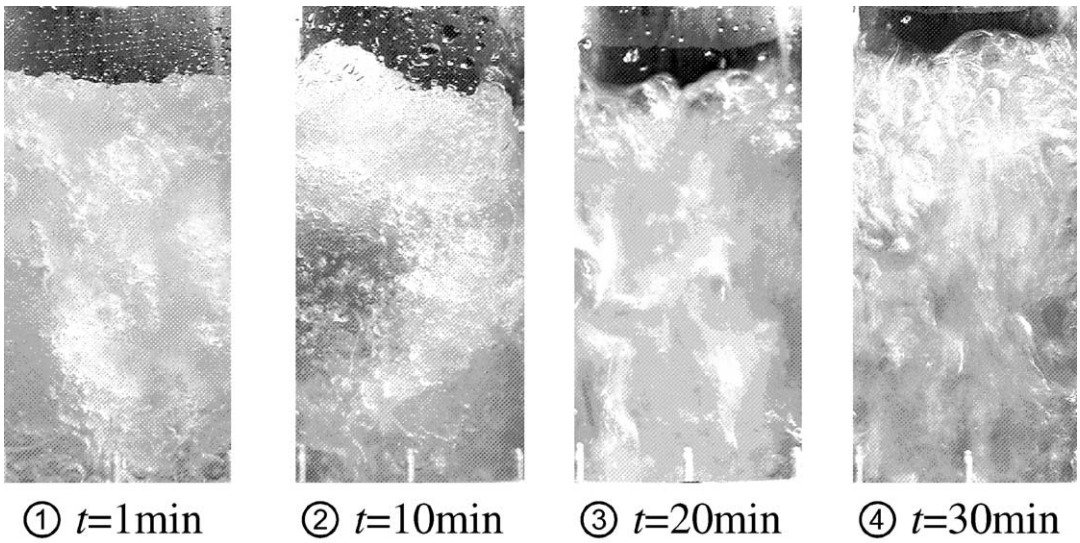

Figure 5. Melting behavior of ice particles with water. (a) View of melting process. (b) Schematic figure of melting condition.

the ice water slurry layer thereby producing condensed water to discharge the latent heat of condensation Φ_c of the vapor. Simultaneously the dry air in the air bubbles covered with the low temperature water in the ice water slurry layer and the aforementioned condensed water is cooled to discharge the sensible heat Φ_s.

Also in the case of ice packing factor $\beta = 0.5$, the whole layer is not fluidized at the beginning of melting as shown in *figure 5(a(1))* and *figure 5(b(1))*. Therefore, volume of water and passage of air bubbles are not enough to fluidize the whole layer. Next, at the initial stage of melting (*figure 5(a(2))*), as shown in *figure 5(b(2))*, melting occurs a little more, and then the surface state of ice water slurry layer changes gradually due to the passage of irregular bubbles generated inside the layer where many slurry ice particles are remaining. After that, at the final stage of melting (*figure 5(a(3))*), as shown in *figure 5(b(3))*, the remaining slurry ice particles change to several lumps. Then, air bubbles combine with one another to wrap up the lumps and change to large air bubbles. And the ice water slurry layer is entirely fluidized. Melting further occurs almost equally over the whole ice water slurry layer (*figure 5(a(4))*), and the increase of the volume of water activates the fluidization of ice water slurry layer. Finally remaining ice particles disappear and change to liquid phase and the melting process is completed.

Figure 6 shows an example of the time history of temperature in ice water slurry layer, temperature and relative humidity of outlet air in the cooling process of ice water slurry. In *figure 6*, it is clear that the characteristic temperature T_c of ice water slurry layer becomes nearly constant at near the melting point T_m ($= 0\,°C$) just after starting warm air injection and that melting of the slurry ice is continued. Then, T_c begins to rise and all the ice particles melt away and change into liquid phase when $t = 45$ min. or so. Finally, the melting process is completed.

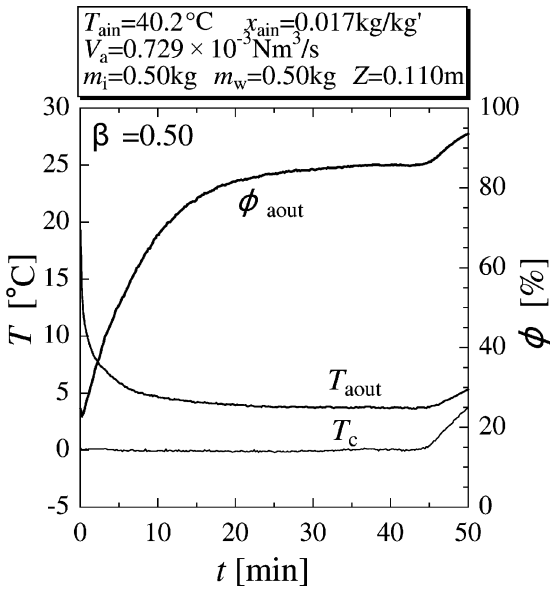

Figure 6. Time histories of outlet air temperature, humidity and ice particle layer temperature.

On the other hand, outlet air temperature T_{aout} from the ice water slurry layer gradually becomes lowered after start of melting, and after lapse of $t = 20$ min. or so, the temperature is relatively stable until completion of melting. This is because the ice water slurry layer is not actively fluidized just after start of melting as shown in *figure 5(a(1,2))*. And the fluidization is activated with the lapse of time, and as a result, T_{aout} gradually becomes lowered close to the level of T_c. After that, as shown in *figure 5(a(3,4))*, the fluidization of the whole ice water slurry layer becomes nearly stabilized and then T_{aout} is relatively stabilized at around 4 °C. And the outlet air temperature T_{aout} increases with increase of the characteristic temperature after all the slurry ice particles are completely melted T_c (when $t = 45$ min. or more).

Also, the outlet air relative humidity ϕ_{aout} from the ice water slurry layer gradually increases after start of melting, and is relatively stabilized at around $\phi_{aout} =$ 85% until completion of melting at $t = 20$–45 min. This is because the fluidization inside the ice water slurry layer is not active just after start of melting, the same as the factor of T_{aout} varying, and it is gradually activated with the lapse of time, and after that, the fluidization of the whole ice water slurry layer is nearly stabilized.

In that case, there are the phenomena of heat transfer and mass transfer between the air bubbles and the ice water slurry. That is, the air bubbles are cooled and condensed, and there are complicated phenomena of heat transfer and mass transfer in the upper surface of the ice water slurry. Then, the outlet air relative humidity ϕ_{aout} from the ice water slurry layer tends to increase gradually. Further, the air bubbles are generated in the ice water slurry layer by warm air passing the dispersion plate and ascend in the ice water slurry layer while changing complicatedly. So, it can be considered that the status in the air bubbles is not uniform at all. Then, all the air bubbles do not reach a status of uniform temperature and uniform humidity by cooling and condensation. Therefore it can be considered that the outlet air relative humidity ϕ_{aout} from the ice water slurry layer does not reach 100% and is stabilized at a point around $\phi_{aout} =$ 85% under the conditions for the present experiment.

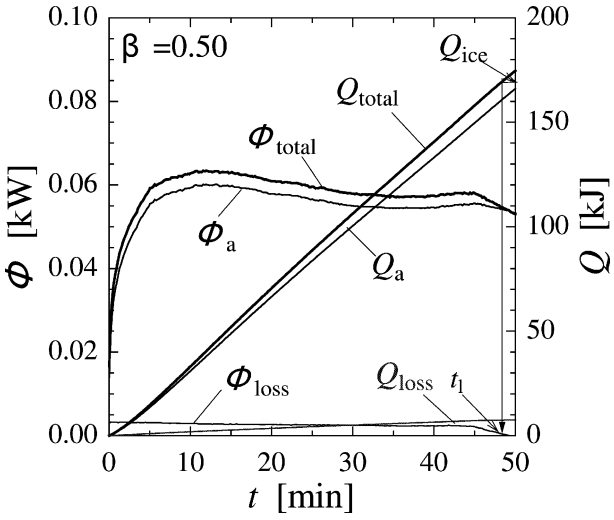

Figure 7. Variation of heat transfer rate with time.

Figure 7 shows the variation of transmitted heat with time in the same case of *figure 6*. As shown in the figure, the time when the time integrated value Q_{total} of the total transmitted heat Φ_{total} in the ice water slurry layer becomes equal to the latent heat Q_{ice} of the ice is defined as the completion time t_l of melting. Then, the transmitted heat Φ_a is calculated from the variation in air enthalpy at the inlet and outlet of the test section. And the time integrated value Q_{total} of the total transmitted heat Φ_{total} is represented by the sum of the time integrated value Q_a of the transmitted heat Φ_a and the time integrated value Q_{loss} of the heat loss Φ_{loss} in the ice water slurry layer. That is, the relations of these can be represented by the following equation (1)–(5).

$$Q_a + Q_{loss} = Q_{total} \tag{1}$$

Here,

$$\Phi_a = V_a/v_{ain}(h_{ain} - h_{aout}) \tag{2}$$

$$h_{ain} = c_{pa} \cdot T_{ain} + (r + c_{ps} \cdot T_{ain})x_{ain} \tag{3}$$

$$h_{aout} = c_{pa} \cdot T_{aout} + (r + c_{ps} \cdot T_{aout})x_{aout} \tag{4}$$

$$Q_{ice} = m_i \cdot L \tag{5}$$

Further, the total transmitted heat Φ_{total} can be represented by the sum of sensible heat Φ_s of the dry air in air bubbles and latent heat of condensation Φ_c of the vapor in air bubbles.

$$\Phi_{total} = \Phi_s + \Phi_c \tag{6}$$

$$\Phi_c = r \cdot V_a/v_{ain} \cdot (x_{ain} - x_{aout}) \tag{7}$$

Here, the heat loss Φ_{loss} was previously calculated from the rate of change in water temperature and test section container wall temperature, when water was filled and left in the test section during stirring. In this way, it has been confirmed that the heat loss Φ_{loss} from the ice water slurry layer to the test section container wall after start of melting is about 5% or less of the total transmitted heat Φ_{total}.

3.3. Characteristics of outlet air temperature

Figure 8 shows the relationship between the maximum temperature efficiency θ and Reynolds number *Re*, where ice packing factor $\beta = 0.25$. Here, the maximum temperature efficiency θ is the nondimensional value of outlet temperature from the test section in the stable region of the outlet temperature and the index of maximum heat exchange performance. Also, the maximum temperature efficiency θ is calculated with respect to the outlet temperature in the stable region of the outlet air temperature ($\pm$0.5 K), and it is defined by the following equation (8).

$$\theta = (T_{ain} - T_{aout})/(T_{ain} - T_m) \tag{8}$$

Also, the Reynolds number *Re* is defined by the following equation (9).

$$Re = U_n \cdot d_n/v_a \tag{9}$$

From *figure 8*, it can be confirmed that the maximum temperature efficiency θ increases with increasing of Reynolds number *Re* in the low Reynolds number region

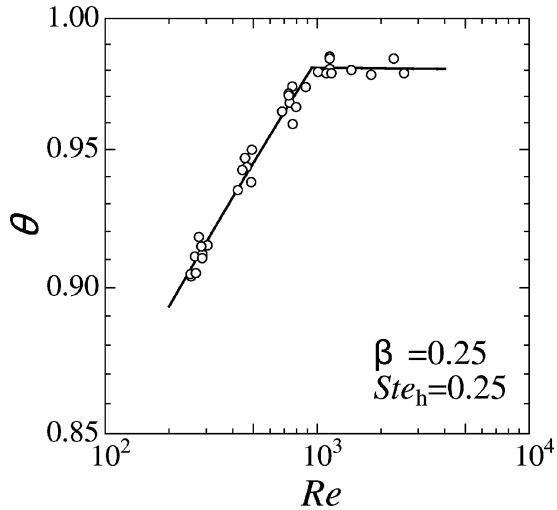

Figure 8. Variation of θ with *Re*.

($Re < 900$). But the maximum temperature efficiency θ is nearly constant even with Reynolds number *Re* increased in the high Reynolds number region ($Re \geq 900$). In the low Reynolds number region ($Re < 900$), the fluidization inside the ice water slurry layer is activated with increasing of *Re*, and promotes the heat transfer between air bubbles and ice water slurry. Therefore, outlet air temperature T_{aout} from the test section decreases and the maximum temperature efficiency θ tends to increase.

On the other hand, the fluidization inside the ice water slurry layer is activated in the high Reynolds number region ($Re \geq 900$). But it can be considered that coefficient of heat transfer between the air bubbles and the ice water slurry nearly reaches the limits and the influence of *Re* increasing on increasing coefficient of heat transfer becomes small in the extreme under the conditions for the present experiments. Consequently, in the high Reynolds number region, the total exchanged heat quantity between the air bubbles and the ice water slurry layer do not vary so much even with increase of air flow velocity, and also outlet temperature T_{aout} from the test section does not vary either. Accordingly, in the high Reynolds number region ($Re \geq 900$), the maximum temperature efficiency θ tends to become nearly constant even with increase of *Re*.

Next, *figure 9* shows the relationship between the maximum temperature efficiency θ and modified Stefan number Ste_{h} that is the nondimensional value of heat capacity of inlet moist air in the stable region of outlet air temperature from the test section. Here, Ste_{h} is defined by the following equation (10).

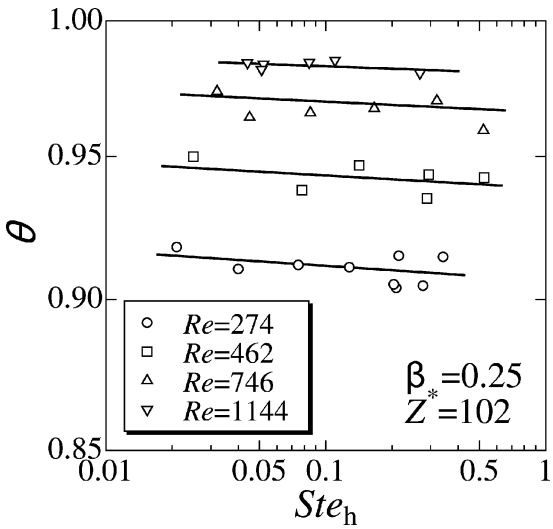

Figure 9. Variation of θ with Ste_{h}.

$$Ste_{\mathrm{h}} = (r + c_{ps} \cdot T_{\mathrm{ain}}) x_{\mathrm{ain}} / L \tag{10}$$

From *figure 9*, it is understood that the maximum temperature efficiency θ tends to slightly decrease with increase of modified Stefan number Ste_{h}. This means that the increase of Ste_{h}, that is, increase of inlet air absolute humidity increases heat capacity $(r + c_{ps} \cdot T_{\mathrm{ain}}) x_{\mathrm{ain}}$ of the moist air bubbles. Then, outlet air temperature after heat exchange with the ice water slurry layer slightly becomes lowered, therefore θ is decreased. Also, regarding the increase of θ with *Re* increased, the tendency is the same as for the consideration in *Figure 7*.

From *figures 8* and *9*, the experimental correlation equation of maximum temperature efficiency θ has been derived by using the root mean square method. In *figure 8*, the maximum temperature efficiency θ does not depend upon the Reynolds number *Re* in the high Reynolds number region ($Re \geq 900$). Taking it into consideration, the experimental correlation equations of θ are as follows, using ice packing factor β, *Re*, Ste_{h} and nondimensional height Z^* of ice water slurry layer.

In applicable range: $252 < Re < 900$

$$\theta = 0.59 \beta^{0.014} Z^{*0.029} Re^{0.056} Ste_{\mathrm{h}}^{-0.004} \tag{11}$$

In applicable range: $900 \leq Re < 2570$

$$\theta = 0.99 \beta^{0.009} Z^{*0.001} Ste_{\mathrm{h}}^{-0.003} \tag{12}$$

Here, the nondimensional height Z^* of ice water slurry layer is defined by the following equation (13).

$$Z^* = Z / d_{\mathrm{n}} \tag{13}$$

From equations (11) and (12), it is clear that the influence of each nondimensional number except Ste_{h} tends to become small and that the influence of Z^* as well as *Re* is extremely reduced in particular in accordance with *Re* changing from the low Reynolds number region ($Re < 900$) to the high Reynolds number region ($Re \geq 900$). Z^* fundamentally influences on staying time of air bubbles inside the ice water slurry layer. So, increase of Z^* means that staying time of air bubbles becomes long. That is, influence of Z^* on θ is recognized in the low Reynolds number region, as shown that index number of Z^* in equation (11) is 0.029. But influence of Z^* on θ becomes small in the high Reynolds number region, as shown that index number of Z^* in equation (12) is 0.001.

However, the influence given to θ by each parameter except *Re* in equations (11) and (12) is very little as

known from each index of equations. That is to say, the influence given to θ by β and Z^* in equation (11) is less than $\pm 2\%$, and the influence given to θ by Ste_h in equation (11) and β, Z^* and Ste_h in equation (12) is as little as less than $\pm 1\%$. Incidentally, the applicable range of β is 0.21–0.84, Z^* is 25–104, Ste_h is 0.04–0.34 and it has been confirmed that the calculated values by equation (11) and (12) coincide with the measured values within deviation of $\pm 4\%$.

3.4. Characteristics of outlet air humidity

Figure 10 shows the time history of outlet air absolute humidity x_{aout} in the aforementioned case of *figure 6*. In the figure, the outlet air absolute humidity x_{aout} in the melting process (stable region) of ice water slurry is smaller than the absolute humidity (0.00503 kg·kg^{-1}) of the saturated air at dry bulb temperature 4 °C. This is because there are the phenomena of heat transfer and mass transfer between the air bubbles and the ice water slurry. That is, the air bubbles are cooled and condensed, and there are complicated phenomena of heat transfer and mass transfer in the upper surface of the ice water slurry. Then, the outlet air relative humidity ϕ_{aout} from the ice water slurry layer tends to increase gradually. Further, the air bubbles are generated in the ice water slurry layer by warm air passing the dispersion plate and ascend in the ice water slurry layer while changing complicatedly. So, it can be considered that the status in the air bubbles is not uniform at all. Then, all the air bubbles do not reach a status of uniform temperature and uniform humidity by cooling and condensation. Therefore it can be considered that the outlet air from the ice water slurry layer does not reach a saturated status at the temperature of the ice water slurry layer.

Next, the relationship between dehumidifying efficiency ε and the modified Stefan number Ste_h, the nondimensional value of inlet air absolute humidity, is shown in *figure 11* where ice packing factor β is 0.26. Here, dehumidifying efficiency ε is calculated from the ratio of difference in inlet and outlet air absolute humidity, that is the ratio of $\Delta x_a (= x_{ain} - x_{aout})$ to the difference $(= x_{ain} - x_o)$ between inlet air absolute humidity x_{ain} and inlet dry air absolute humidity $x_o (= 0$ kg·kg$^{-1})$. That is, it is defined by the following equation.

$$\varepsilon = (x_{ain} - x_{aout})/(x_{ain} - x_o) \tag{14}$$

As is shown in the figure, there is such a tendency that ε increases rapidly in the range of $Ste_h < 0.085$, but the increasing rate of ε decreases when $Ste_h \geq 0.085$ and ε gradually comes close to $\varepsilon = 1$. From equation (10), increasing of Ste_h means increasing of inlet air absolute humidity x_{ain} or inlet air temperature T_{ain}. When Ste_h is relatively small, that is, x_{ain} is relatively small, increasing of x_{ain} has influenced on increasing of ε $(= 1 - x_{aout}/x_{ain})$. Therefore ε is much more dependent on Ste_h. However, it can be considered that when x_{ain} becomes relatively large and Ste_h exceeds the point around 0.1, the increasing tendency of x_{ain} against ε gradually becomes less and ε comes close

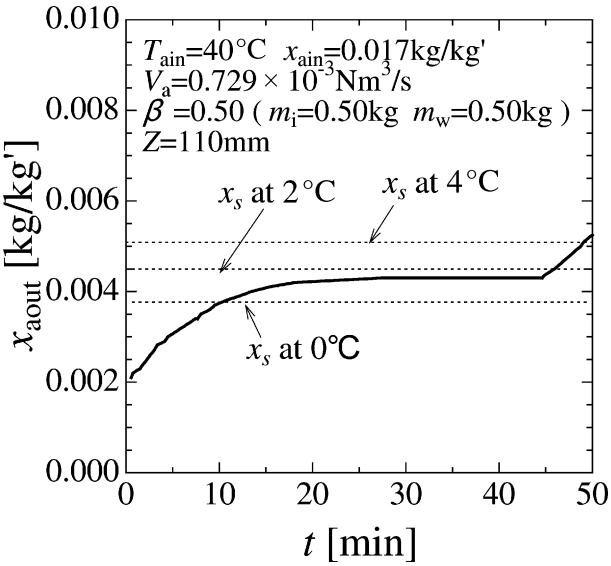

Figure 10. Time history of outlet air absolute humidity.

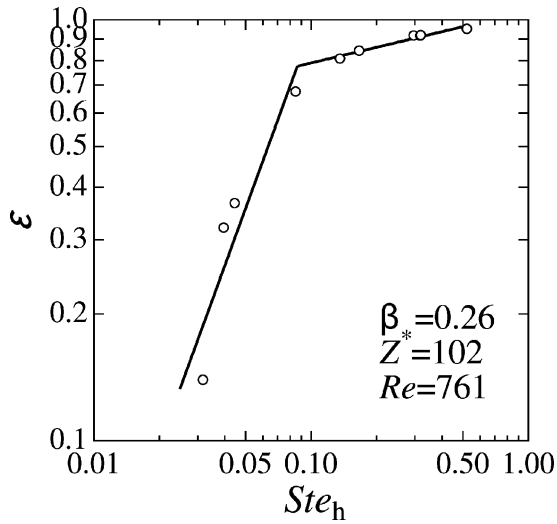

Figure 11. Variation of ε with Ste_h.

to $\varepsilon = 1$. Accordingly, the result of nondimensional arrangement of ε from the above-mentioned relations by using ice packing factor β, nondimensional height Z^* of ice water slurry layer, Re and Ste_h can be represented by the following experimental correlation equations.

In applicable region: $0.03 < Ste_h < 0.085$

$$\varepsilon = 28\beta^{0.049} Z^{*0.0067} Re^{0.0091} Ste_h^{1.5} \tag{15}$$

In applicable region: $0.085 \leq Ste_h < 0.50$

$$\varepsilon = 1.1\beta^{0.049} Z^{*0.0067} Re^{0.0091} Ste_h^{0.18} \tag{16}$$

The following characteristics can be quantitatively represented by the equations (15) and (16). That is, the increase of Ste_h and Re results in the increase of ε due to the increase of inlet air heat capacity $(r + c_{ps}T_{ain})x_{ain}$ and heat transfer between ice water slurry and air.

Also, with increase of ice packing factor β and the nondimensional height Z^* of ice water slurry layer, the contact length of air bubbles with ice water slurry layer is increased. This behavior is allowed to increase the maximum temperature efficiency θ and to lower the outlet air temperature T_{aout}. Accordingly, there is a tendency that ε is slightly increased with increase of β and Z^*.

However, an influence of each parameter except Ste_h on ε is small in the extreme, as known from each index in equations (15) and (16). Incidentally, the applicable range of β is 0.15–0.84, Z^* is 25–105, Re is 252–1169 and it has been confirmed that the calculated values by equations (15) and (16) coincide with the measured values within deviation of ±10%.

3.5. Characteristics of completion time of melting

In the case of cooling equipment by direct contact heat exchange as mentioned in this study, it is difficult to obtain accurately the heat transfer characteristics since the heat transfer contact area between ice water slurry layer and warm air cannot be measured. Therefore, instead of heat transfer characteristics, the characteristics of the completion time of melting have been examined. The completion time t_l of melting is determined by the amount of heat given by the injected warm air to the ice water slurry layer, and it is possible to make the arrangement by using the difference in enthalpy between inlet and outlet air. However, when putting such cooling equipment by direct contact heat exchange to practical use, it will be effective if the completion time t_l of melting t_l can be estimated only from the inlet air conditions. Accordingly, the relationship between transmitted heat Φ_a and completion time t_l of melting can be indirectly expressed by showing the relations of inlet air condition and completion time t_l of melting. So, the relationship between the nondimensional completion time t_l^* of melting and ice packing factor β is shown in *figure 12*. Here, definition about the nondimensional completion time t_l^* of melting is the nondimensional value to represent the completion time of melting as in equation (17) [7]. In the equation (17), d_n is diameter of circular nozzle located on the dispersion plate, $d_n = 2{\cdot}10^{-3}$ m and a_a is thermal diffusivity of air.

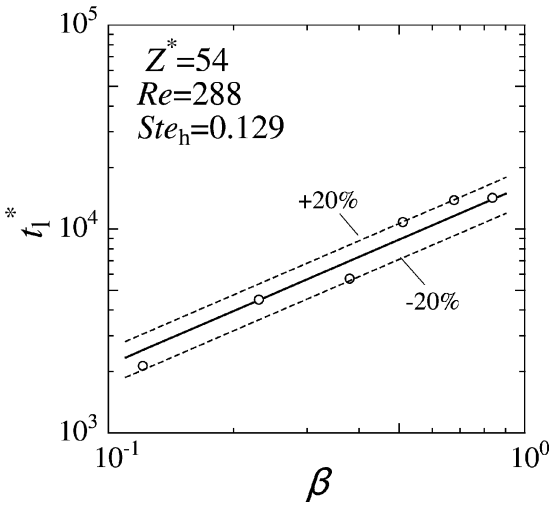

Figure 12. Variation of t_l^* with β.

$$t_l^* = t_l \cdot a_a / d_n^2 \tag{17}$$

As is shown in *figure 12*, there exists a tendency that the nondimensional completion time t_l^* of melting increases with an increase of ice packing factor β.

This behavior of t_l^* is explained by the fact that the latent heat of the ice in the ice water slurry layer increases as ice packing factor β is increased, and consequently the completion time t_l of melting increases.

Next, the relationship between the nondimensional completion time t_l^* of melting and modified Stefan number Ste_h that is the nondimensional value of heat capacity of inlet moist air is shown in *figure 13*. As shown in this figure, t_l^* tends to be shortened with increasing Ste_h. Since the increase of Ste_h, that is, the increase of inlet air absolute humidity is allowed to increase heat capacity $(r + c_{ps} \cdot T_{ain})x_{ain}$ of moist air bubbles, the

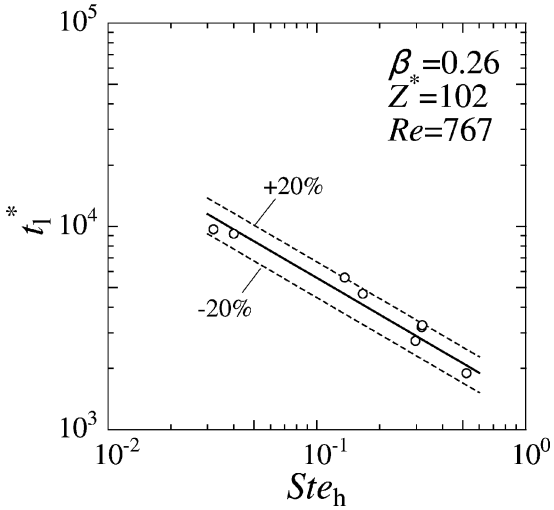

Figure 13. Variation of t_l^* with Ste_h.

amount of latent heat exchange between fine ice particles and warm air increases, and as a result, t_l^* becomes short.

From the above-mentioned relations, the nondimensional arrangement of the nondimensional completion time t_l^* of melting was performed with the use of ice packing factor β , the nondimensional height Z^* of ice water slurry layer, Re and Ste_h. The result can be represented by the following experimental correlation equation.

$$t_l^* = 8.9 \cdot 10^3 \beta^{0.87} Z^{*1.0} Re^{-0.80} Ste_h^{-0.60} \qquad (18)$$

From the equation (18), the following characteristics can be quantitatively represented. That is, the increase of β and Z^* against t_l^* tends to make t_l^* longer because the amount of latent heat and the contact length of air bubbles with the ice water slurry layer are increased. On the contrary, when Re increases, t_l^* tends to be shortened since the fluidization in the ice water slurry layer is activated and coefficient of heat transfer is improved. Also, t_l^* tends to be shortened with increase of Ste_h, because the latent heat of vapor condensation of the inlet air increases and the melting of ice water slurry layer is promoted. Incidentally, the applicable range of β is 0.25–0.84, Z^* is 25–102, Re is 252–1169, Ste_h is 0.04–0.34 and it has been confirmed that the calculated values by equation (18) coincide with the measured values within deviation of $\pm$20%.

4. CONCLUSION

The present study has dealt with the characteristics of melting by injecting warm air to ice water slurry layer that is the mixture of ice particles and water as the latent heat storage material to obtain low temperature air and low humidity air by direct contact heat exchange with the ice water slurry layer. As a result, the following conclusion has been obtained.

First, about fluidization of layer and air bubbles, in the case of only ice particles layer (ice packing factor $\beta = 1.0$) packed into the test section, the layer is not entirely fluidized because of little water at the early stage of melting. But in the case of ice water slurry layer, the whole layer is fluidized relatively earlier, then the ice particles in the ice water slurry change into several lumps and the air bubbles combine one another to wrap up the lumps and change to large bubbles. Thus, the ice water slurry layer is entirely fluidized.

Secondly, about characteristics of outlet air temperature, the fluidization in the ice water slurry layer is activated with increase of Re when $Re < 900$, then the maximum temperature efficiency θ increases. But θ tends to become nearly constant when $Re \geq 900$. This is because coefficient of heat transfer between the air bubbles and the ice water slurry nearly reaches the limits and the influence of Re increasing with increase in coefficient of heat transfer becomes small in the extreme.

Thirdly, about characteristics of outlet air humidity, the dehumidifying efficiency ε tends to increase due to the increase of heat capacity of inlet moist air and the promotion of heat transfer in accordance with the increase of modified Stefan number Ste_h and Re.

Finally, about characteristics of completion time of melting, the nondimensional completion time t_l^* of melting, that represents the completion time t_l of melting, tends to increase according to the increase of ice packing factor β and nondimensional height Z^* of ice water slurry layer and to decrease according to the increase of Reynolds number Re and modified Stefan number Ste_h. And the experimental correlation equation of t_l^* can be derived as the function of β, Z^*, Re and Ste_h.

REFERENCES

[1] Takemoto K., Sakai K., Proceeding of SHASE Annual Conference (1996) pp. 717–720.

[2] Kakutani S., Abiru K., Watanabe M., Kawata A., Cyo N., Watanabe T., Mitsubishi Heavy Industries Technical Report 33-2 (1996) 114–117.

[3] Inaba H., Horibe A., Ozaki K., Yokota M., Study of cold heat energy Release characteristics of flowing ice water slurry in a pipe, Trans. JSRAE 14 (3) (1997) 265–276.

[4] Ohira A., Yanadori M., Iwabuchi K., Kimura T., Tsubota Y., Cold energy release characteristics of ice/air direct contact heat exchanger, Trans. Japan Soc. Mech. Engrg. B 65 (633) (1999) 1743–1751.

[5] Inaba H., Morita S., Fundamental study on cold energy storage and energy release systems of fine capsulated latent-heat storage material-water mixture, Trans. Japan Soc. Mech. Engrg. B 61 (592) (1995) 4448–4455.

[6] Inaba H., Sato K., Fundamental study on latent cold heat storage by means of oil droplets with low freezing point, Trans. Japan Soc. Mech. Engrg. B 62 (602) (1996) 3704–3711.

[7] Inaba H., Horibe A., Haruki N., Tsukamoto H., Kim M., Proceeding of 36th Japan Heat Transfer Symposium 1 (1999) pp. 55–56.